PUBLISHED BY IOP PUBLISHING FOR SISSA MEDIALAB

RECEIVED: *October 18, 2014*
ACCEPTED: *November 19, 2014*
PUBLISHED: *???, 2014*

16th INTERNATIONAL WORKSHOP ON RADIATION IMAGING DETECTORS
22–26 JUNE 2014,
TRIESTE, ITALY

Laser mapping of the inter-strip response in double sided silicon strip detectors for particle identification

A. Castoldi,[a,b] **C. Guazzoni,**[a,b,1] **T. Parsani,**[a,b] **F. Riccio**[a,b] **and P. Zambon**[a,b,2]

[a] *Dipartimento Elettronica, Informazione e Bioingegneria, Politecnico di Milano, Piazza Leonardo da Vinci, 32, 20133 Milano, Italy*
[b] *INFN, Sezione di Milano, Via Celoria, 16, 20133 Milano, Italy*

E-mail: Chiara.Guazzoni@mi.infn.it

ABSTRACT: Silicon microstrips are widely used in nuclear physics experiments when high granularity and high resolution is required (e.g. particle-particle correlation). In addition microstrip detectors are used in the field of X-ray detection for position resolved X-ray spectroscopy. In the framework of the construction of a novel Femtoscope ARray for Correlation and Spectroscopy, named FARCOS, we are performing a thorough characterization of the silicon detector layers in terms of the efficiency and charge collection properties as a function of the point of incidence and type of interaction. We have experimental evidence — as previously observed also in the literature for other strip detectors — that inter-strip incidence alters the signal shape not only for the trivial charge division but also affecting the shape of the induced signal on neighbor strips. The phenomenon can be more or less pronounced depending on the energy and ion type but it is always present. In order to surgically probe the response of the inter-strip region we tested the detector both in back and in front injection with an infrared pulsed laser at two different wavelengths (705 nm and 904 nm). Depending on the side of interaction, on the position of incidence and on the absorption length, the shapes of the induced signals are significantly altered and signals of opposite polarity or bipolar signals arise. In order to get a complete picture of the physical phenomena at the basis of the aforementioned behavior we performed detailed 3D device simulations with a custom semi-analytical code and compared the results with the experimental data. The paper focuses on the description of the experimental measurements and their exhaustive description and interpretation.

KEYWORDS: Si microstrip and pad detectors; Particle identification methods; Detector alignment and calibration methods (lasers, sources, particle-beams)

[1] Corresponding author.
[2] Now with Dectris Ltd., Baden, Switzerland.

doi:xxxxxxx

Contents

1 Introduction

Silicon microstrips are widely used in nuclear physics experiments when high granularity and high resolution of the detection system are required, as, for example in particle-particle correlation measurements [1–4]. In addition, microstrip detectors are used in the field of X-ray detection for position-resolved X-ray spectroscopy [5–8].

A novel Femtoscope ARray for Correlation and Spectroscopy, named FARCOS [2], is being constructed aiming to perform the identification in charge and mass of particles stopping even in the first detection layer (by means of pulse shape analysis). It should feature high angular and energy resolution and be able to reconstruct the particle's momentum at high precision. Each telescope features an active area of 6.4 cm $\times$ 6.4 cm and is composed of three detection stages. The first ΔE stage is a Double Sided Silicon Strip Detector (DSSSD), 300 μm thick, featuring 32 $\times$ 32 strips. The second ΔE stage is again a DSSSD, 1500 μm thick, featuring 32 $\times$ 32 strips. Four CsI(Tl) crystals with an active area of 3.2 cm $\times$ 3.2 cm and an absorption length of 6 cm — arranged in window mode — act as calorimeter.

The goal of particle identification by means of pulse shape analysis requires a thorough characterization of the silicon detector layers in terms of the efficiency and collection properties as a function of the point of incidence. We have experimental evidence — also reported in literature for other strip detectors [9–14] — that incidence in the gap between two strips not only causes trivial charge division but also alters the shape of the induced signal. Furthermore the phenomenon depends significantly on the energy and ion type.

We performed a systematic investigation [15] of the impact on the induced signal shape of particle interaction in the inter-strip region by exploiting as probing tool, a pulsed monochromatic ion beam [16, 17] — featuring an average number of particles per pulse well below one per bunch — with high energy and spatial resolution. However, the spatial definition of the particle beam was

not enough to surgically probe the detector response at every position along the inter-strip gap, so as to compare measurements and simulations. Therefore, we tested the detector both in back and in front injection with an infrared pulsed laser at two different wavelengths (705 nm and 904 nm) in order to surgically probe the response of the inter-strip region.

2 The detection system: DSSSD, front-end and DAQ

2.1 Double-Sided Silicon Strip Detector

The detector used in the present characterization is 300 μm thick and double side orthogonally segmented in strips. It is manufactured by Micron Semiconductor Ltd (U.K.), according to the standard BB7(DS) design. It features 64 mm $\times$ 64 mm active area, 2 mm strip pitch on both sides and, therefore, 32 strips per side. The strips are DC coupled. The bulk material is n-type doped (FZ Silicon, with a resistivity of 3 kΩcm — factory data). Strips are covered by 300 nm Aluminium layer. Ten guard rings left floating surround the detector active area. The inter-strip gap on the junction-side is 25 μm, while the inter-strip gap on the ohmic-side, as visible in figure 1, features a more complicated structure, with an overall length of 40 μm — the central 15 μm of the inter-strip region feature a shallow p+ implantation to improve strips isolation. The detector chip is mounted on an FR4 frame and Kapton flex cables — about 20 cm long — are wedge bonded to the strips on one end and have SAMTEC SSQ-117-22-G-D-RA 34 poles connectors on the other end. The measured strip bulk capacitance is 41 pF at the depletion voltage, while the inter-strip capacitance (single-side contribution) is 12 pF (comprising the contribution of the Kapton cable). The measured bulk resistivity — extracted from the C-V measurements — is 19 kΩcm.

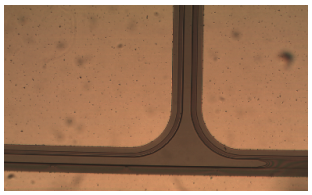

Figure 1. Microphotograph of the inter-strip region on the ohmic-side close to the guard region.

2.2 Analogue front-end

The front-end is an hybrid large-bandwidth charge preamplifier with pseudo-differential output, assembled in compact modules housing 32 channels each. Figure 2 shows the block diagram of the designed front-end. The input transistor is a high-transconductance JFET, whose bias current is chosen as a compromise between power dissipation and noise performance. A low-capacitance analogue switch allows digital selection of the gain even during operation. A class AB low-distortion output stage is provided prior to the output buffer — based on an operational amplifier — to ensure the maximum dynamic range for signals of both polarity.

For the second phase of the project, the final system will foresee 16 telescopes, i.e. 2048 output channels for the DSSSDs, VLSI design is under way in 0.35 μm AMS CMOS technology.

2.3 Digital DAQ

The signals coming from the charge preamplifiers are fed to custom anti-aliasing amplifiers (AAAs) with adjustable gain and bandwidth. We modified a previous design of AAAs [18] to receive the differential signals coming from the charge preamplifiers. A standard single-unit 16-channel NIM module provides in a single device: i) a second order anti-aliasing filter with two programmable cutting frequencies (8 MHz and 40 MHz); ii) a programmable-gain amplifier (gains of $1\times$, $2\times$, $4\times$, $8\times$) to cope with the full dynamic range of the ADC, able to select the polarity of the output signal by means of an inverting or non-inverting circuit; iii) a programmable output offset voltage with AC or DC input coupling selection.

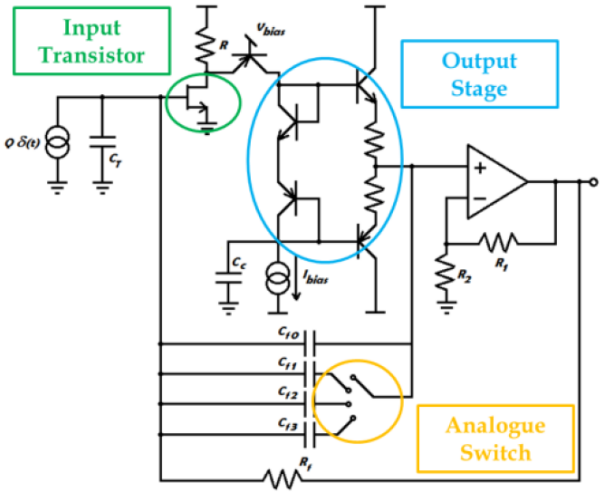

Figure 2. Block diagram of the designed front-end with selectable gain.

Figure 3 shows the scheme of principle of the digital Data Acquisition System and of the Control Software. For every strip, the amplified waveform is digitized by eight SIS3301 SADC boards at a sampling frequency of 100 MS/s. The trigger signal from the laser is distributed to all SADC boards by means of Logic Fan-in / Fan-Out. After each trigger, a single event is transferred through an optical fibre link by the VME/PCI bridge, then acquisition is restarted. A dedicated software module controls the acquisition and stores the digitized waveforms into permanent storage.

3 Experimental qualification

In order to perform a systematic investigation of the impact of charge generation in the inter-strip region on the induced signal shape we finely mapped the detector response in the inter-strip region with a focused infrared pulsed laser. Different laser wavelengths, have been tested mimicking different ionization profiles. The laser excitation features an ionization profile different from particles (exponential absorption instead of Bragg peak charge generation), but the chosen wavelengths (704 nm and 905 nm) are an adequate, well controllable and reproducible tool to probe the phenomenon. In addition we decided to digitize the whole output waveform at all strips of the junction and ohmic side at each acquisition in order to have the possibility to study the induction process in detail.

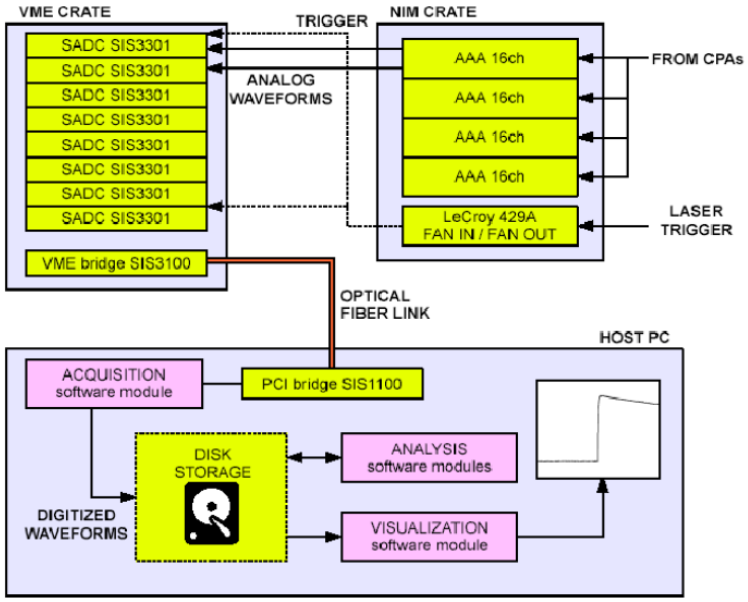

Figure 3. Scheme of principle of the digital Data Acquisition System and of the Control Software.

3.1 Experimental setup

One DSSSD prototype (300 μm thick) has been mounted and tested at room temperature in air. Figure 4 shows the photograph of the experimental setup with the microstrip detector mounted in the laser test suite. An infrared pulsed laser at two different wavelengths (705 nm — absorption length 6.4 μm — and 904 nm — absorption length 37 μm) has been used in order to probe different ionization profiles. The pulse duration of less than 1 ns and the spot size of less than 10 μm FWHM are well suited to probe the inter-strip region. The laser spot was focused by means of microscope optics on the ohmic-side (back-side injection) and on the junction-side (front-side injection) of the detector to generate the signal charge and test the detector response matrix at different bias voltages. Since the strips are covered by Aluminium for a large fraction of the area, it was possible to probe just the area close to the inter-strip region. The width of the naked Silicon strip is large enough to ensure full collection of the generated charge on a single strip for the first irradiation point during the scan. Profiting of the high spatial resolution of the laser spot we performed several scans across the strips to record the waveform response and to investigate their shape as a function of the position of interaction, as schematically shown in figure 5.

We recorded a set of waveforms pertaining to the two neighbour strips of each detector side facing the inter-strip region under study. For every incidence point of the laser spot we averaged the recorded waveforms in order to improve the signal-to-noise ratio, then we extracted the maximum positive value (MAX, always positive) and the minimum negative value (MIN, always negative) from the baseline-subtracted averaged waveforms.

3.2 Inter-strip response mapping

For sake of brevity we limit here to the case of the 705 nm wavelength that features a higher ionization density located close to the injection surface and, therefore, better highlights all the

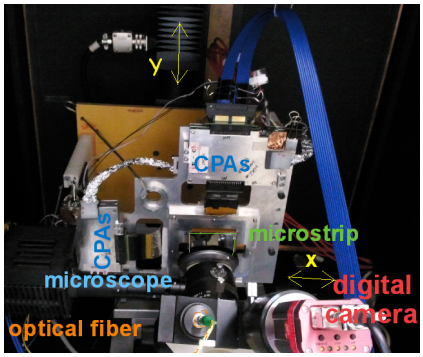

Figure 4. Photograph of the experimental setup with the microstrip detector mounted in the laser test suite.

Figure 5. Schematic illustration of the laser scans (indicated with black arrows) performed to study the phenomenology of inter-strip events (a) front-side injection; (b) ohmic side injection.

phenomena. In all the measurement shown here the detector was biased at 5 V over-depletion (i.e. at -25 V). Figure 6 shows the measured output waveforms as a function of the irradiation point when the detector was mounted in front injection and the laser was focused in correspondence of the inter-strip region of the ohmic side (scan marked as B in figure 5a). The two adjacent strips of the junction side ((a) and (b)) and the two adjacent strips of the ohmic side ((c) and (d)) closer to the interaction point are shown. No signal is measured at strips farther from the interaction point. Since the signal is measured with an inverting charge preamplifier, p+ strips collecting holes will show a negative pulse, while the output signal at ohmic strips — collecting electrons — is positive. The asymptotic value of the induced charge is a measure of the net collected charge. As it can be noticed, when the laser spot moves from strip j to strip $j+1$ and enters the inter-strip region not only the charge collected at the p+ strip j decreases and the one at the p+ strip $(j+1)$ increases as expected for trivial charge sharing, but also a small and fast peak of opposite polarity arises. In addition once the peak vanishes the output waveform does not perfectly return to zero, but a non-zero value is measured when the transient is off. The shape of the measured signal is affected by the behavior of the weighting field pertaining to the two strips, according to the Ramo theorem [19] and to plasma effect. Let's focus on the behavior of the signals moving from strip j toward the center of the inter-strip region. The other signals will exhibit a perfectly symmetrical behavior.

The observed shape can be justified as follows. When the laser spot is impinging on strip j full collection is achieved on the same strip and strip $(j+1)$ sees no signal, however in our case we are irradiating at the rim of the strip — due to the presence of the Al coating — and, therefore a tiny fraction of the generated charge already spreads in the inter-strip region. The weighting potential of strip $(j+1)$ extends to that region. As a consequence p+ strip j always sees

holes approaching and electrons moving away, while strip $(j+1)$ at the first time instants after plasma erosion experiences holes moving away towards strip j and electrons coming closer and only afterwards holes approaching and electrons going away, giving rise to the signal of opposite polarity. The small offset is due to the (small) fraction of charge trapped in the potential pocket that forms in the inter-strip region.

The slight increase of the amplitude of the signal measured at the ohmic side strips is due to the effect of the residual halo of the laser spot, but does not impact on the significance of the measurement.

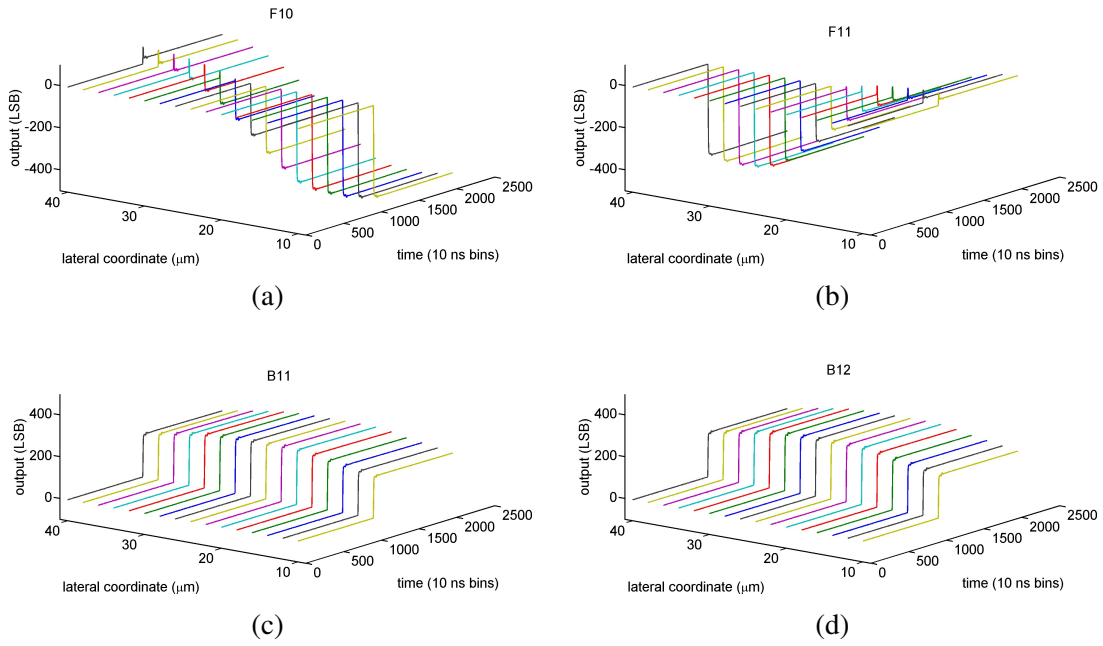

Figure 6. Measured output waveforms recorded at different position of impact in the case of 705 nm laser irradiation in front injection at two adjacent strips of the junction side ((a) and (b)) and of the ohmic side ((c) and (d)). The detector was biased at 5 V over-depletion.

Figure 7 shows the corresponding waveforms in the case of back injection in the same experimental conditions. The peculiar shape of the weighting potential of the ohmic side strips, related to the structure of the inter-strip region (see section 2.1) causes higher fast peak of opposite polarity. In this case, in addition the charge loss on the front side strips is evident and becomes more pronounced approaching the center of the inter-strip region.

4 Conclusions

We performed a detailed study of the impact of inter-strip incidence on the shape of the output signals in microstrip detectors. The characterized detector is one of the Silicon layers of the FARCOS telescope, being built for correlation and spectroscopy in nuclear physics experiments.

In order to surgically probe the response of the inter-strip region we tested the detector response matrix both in back and in front injection with an infrared pulsed laser at two different

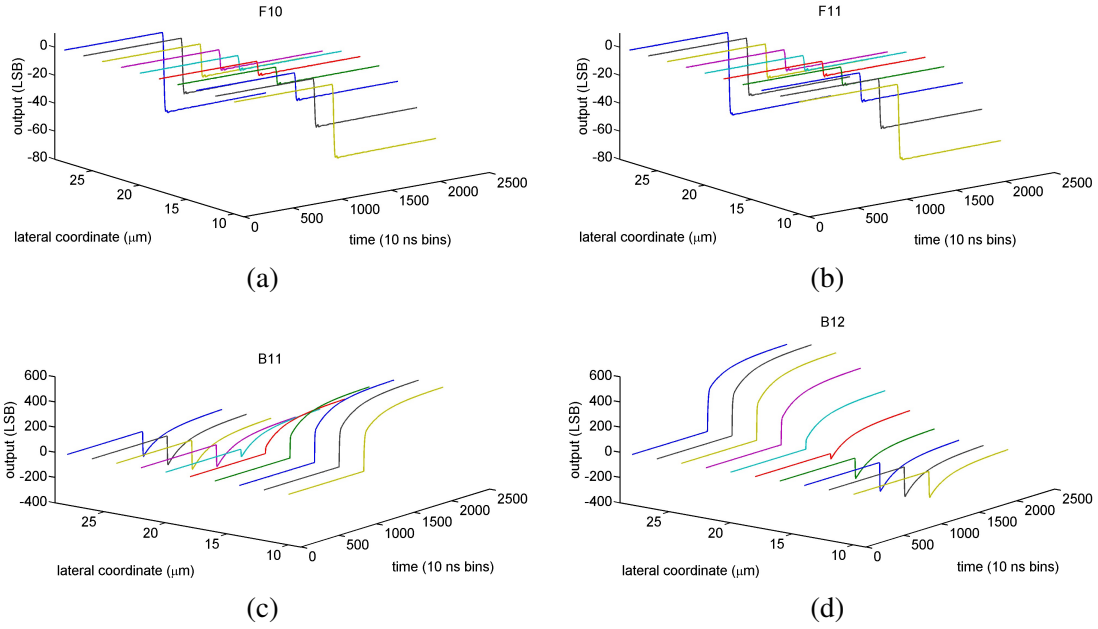

Figure 7. Measured output waveforms recorded at different position of impact in the case of 705 nm laser irradiation in back injection at two adjacent strips of the junction side ((a) and (b)) and of the ohmic side ((c) and (d)). The detector was biased at 5 V over-depletion.

wavelengths (705 nm and 904 nm). We could correlate the shape of the induced signals — according to the position of interaction — to the shape of the weighting field of the two strips closer to the interaction point. Depending on the side of interaction, on the position of incidence and on the absorption length, the shapes of the induced signals are significantly altered and signals of opposite polarity or bipolar signals arise. In no cases signals with the opposite polarity can be ascribed to collection of opposite sign charges by the corresponding strip as sometimes reported in the literature. In addition significant charge loss can occur for incidence in the inter-strip region that increases the unwanted background limiting particle identification capability, especially at low deposited energy.

Acknowledgments

The FARCOS project is being developed in the framework of the INFN (Istituto Nazionale di Fisica Nucleare) EXOCHIM experiment and of the MIUR (Ministero dell'Universita' e della Ricerca Scientifica) program PRIN2009, protocol 2009RLCYL8, October 17, 2011 – October 17, 2013.

The authors gratefully acknowledge the FARCOS collaboration, composed by the following institutions: INFN (Sezione di Catania, Laboratori Nazionali del Sud, Gruppo Collegato di Messina, Sezione di Milano, Sezione di Napoli), Universita' degli Studi di Catania (Dip. di Fisica e Astronomia), Universita' degli Studi di Messina (Dip. di Fisica), Politecnico di Milano (Dip. Elettronica, Informazione e Bioingegneria), Università di Napoli Federico II (Dip. di Fisica), Universita' di Enna Kore, Univesidad de Huelva (Departamento de Física Aplicada) and IN2P3, CNRS and Sergio Masci (Politecnico di Milano) for his ability in detector bonding.

References

[1] G. Verde et al., *Correlations and characterization of emitting sources*, *Eur. Phys. J.* **A 30** (2006) 81.

[2] G. Verde et al., *The Farcos project: Femtoscope Array for Correlations and Femtoscopy*, *J. Phys. Conf. Ser.* **420** (2013) 012158.

[3] E. Pollacco et al., *MUST2: A new generation array for direct reaction studies*, *Eur. Phys. J.* **A 25** (2005) 287.

[4] M.S. Wallace et al., *The high resolution array (HiRA) for rare isotope beam experiments*, *Nucl. Instrum. Meth.* **A 583** (2007) 302.

[5] A. Bergamaschi et al., *The MYTHEN detector for X-ray powder diffraction experiments at the Swiss Light Source*, *J. Synchrotron Rad.* **17** (2010) 653.

[6] D. Protic et al., *Two-dimensional Microstrip Germanium Detector for the spectroscopy of hard X-ray transitions*, *IEEE Trans. Nucl. Sci.* **52** (2005) 3194.

[7] H. Youn et al., *X-ray interaction-induced signal and noise performances of edge-on silicon microstrip detectors for digital mammography*, 2011 *JINST* **6** C11004.

[8] E. Del Monte et al., *An X-ray imager based on silicon microstrip detector and coded mask*, *Nucl. Instrum. Meth.* **A 576** (2007) 191.

[9] J. Yorkston et al., *Interstrip surface effects in oxide passivated ion-implanted silicon strip detectors*, *Nucl. Instrum. Meth.* **A 262** (1987) 353.

[10] S. Takeda et al., *Development of double-sided silicon strip detectors (DSSD) for a Compton telescope*, *Nucl. Instrum. Meth.* **A 579** (2007) 859.

[11] Y. Blumenfeld, *MUST: A silicon strip detector array for radioactive beam experiments*, *Nucl. Instrum. Meth.* **A 421** (1999) 471.

[12] J. Hayward and D. Wehe, *Incomplete charge collection in an HPGe double-sided strip detector*, *Nucl. Instrum. Meth.* **A 586** (2008) 215.

[13] D. Torresi et al., *Influence of the interstrip gap on the response and the efficiency of Double Sided Silicon Strip Detectors*, *Nucl. Instrum. Meth.* **A 713** (2013) 11.

[14] L. Grassi et al., *Anomalous behaviour of DSSSDs*, *AIP Conf. Proc.* **1491** (2012) 135.

[15] A. Castoldi et al., *Experimental Investigation of the Impact of Inter-Strip Incidence on the Signal Shape in Double Sided Silicon Strip Detectors for Particle Identification*, *IEEE Nucl. Sci. Symp. Med. Imag. Conf. Rec.* **2013** (2013) 1.

[16] F.A. Mirto and L. Carraresi, *The pulsed beam facility at the Tandetron accelerator in Florence*, *Nucl. Instrum. Meth.* **B 266** (2008) 2113.

[17] A. Castoldi et al., *Upgrade of the DeFEL Proton Beamline for Detector Response Mapping*, *IEEE Nucl. Sci. Symp. Med. Imag. Conf. Rec.* **2013** (2013) 1.

[18] C. Boiano et al., *A 16-Channel Programmable Antialiasing Amplifier*, *IEEE Nucl. Sci. Symp. Conf. Rec.* **2010** (2010) 1389.

[19] S. Ramo, *Currents Induced by Electron Motion*, *Proc. IRE* **27** (1939) 584.